

ND280 Simulation Studies

Adam D. Schneider

TRIUMF Neutrino Group
Vancouver, British Columbia

Simon Fraser University
Mathematical Physics
20005-1270

May 4, 2004

Contents

1	Neutrino Physics	3
2	The T2K Project	4
3	ND280m Design	6
3.1	Cerenkov Radiation	6
3.2	Scintillators	7
3.3	Wavelength Shifters	8
3.4	Photomultiplier Tubes	8
4	Simulation Studies	8
4.1	Purpose	8
4.2	GEANT3 Configuration	10
4.3	Data Set 1	13
4.3.1	Setup	13
4.3.2	Results	15
4.3.3	Conclusions	21
4.4	Data Set 2	21
4.4.1	Setup	21
4.4.2	Results	23
4.4.3	Conclutions	33
4.5	Quasi-Elastic Recoiled Proton Distribution	35
4.5.1	Introduction	35
4.5.2	Results	36
4.5.3	Conclusions	38
4.6	Summary of Conlusions / Recomendations	38

1 Neutrino Physics

Wolfgang Pauli first hypothesized the existence of a tiny neutral particle in 1930, as a means of explaining the apparent non-conservation of energy and momentum in nuclear β -decay. This hypothesized particle was considered to be massless (or of mass far below the measurable threshold) and was named the ‘neutrino’ by Enrico Fermi, meaning ‘little neutral one’. The first evidence for the existence of a neutrino did not come for another 26 years, and had a tremendous impact on particle physics and the development of the Standard Model. By 1989 it had been confirmed that there are in fact three distinct types (or flavors) of neutrinos each paired with its respective lepton: electron, muon and tau neutrinos.

As the neutrino began filling in the gaps of the latest theories, it was calculated that the sun was in fact producing a flux of about 10^{14} neutrinos per square meter every second. More specifically it is electron neutrinos that are produced by the sun, and conveniently these were the easiest type of neutrino to identify. It was in 1964 in the chlorine detector of Ray Davis’ Homestake Mine experiment that the first solar neutrinos were detected, but there was a problem. The number of electron neutrinos observed was drastically less than that predicted. Since our model of the sun had done so well thus far, this ‘Solar Neutrino Problem’ suggested that the error was in our understanding of the neutrino. This prompted the idea that the neutrinos may be changing type on route to the earth (flavor oscillations). By 2001, a comparison of data from the Sudbury Neutrino Observatory (SNO) and Super-Kamiokande (Kamioka Nucleon Decay Experiment), had strong evidence that solar neutrinos do in fact oscillate and in turn must have some finite mass. There was also evidence of neutrino oscillations coming from the nuclear reactor neutrinos in the KAMLAND experiment.

By 1999 the worlds first long-baseline neutrino experiment had begun in Japan, in hopes of more accurately defining the characteristics of the neutrinos and their behavior. K2K (KEK to Kamioka) used the KEK 12GeV proton synchrotron to generate a neutrino beam that would travel hundreds of kilometers to the Super-K detector in Kamioka. The K2K project was logging enough events to confirm the neutrino oscillations, but to get more information about the neutrino a more powerful synchrotron will be needed. This synchrotron is now being replaced by a 50GeV proton synchrotron that will be constructed at the Japan Atomic Energy Research Institute (JAERI) in Tokai (shown in figure 1), giving way to one of the newest and largest scale neutrino projects in history-T2K.

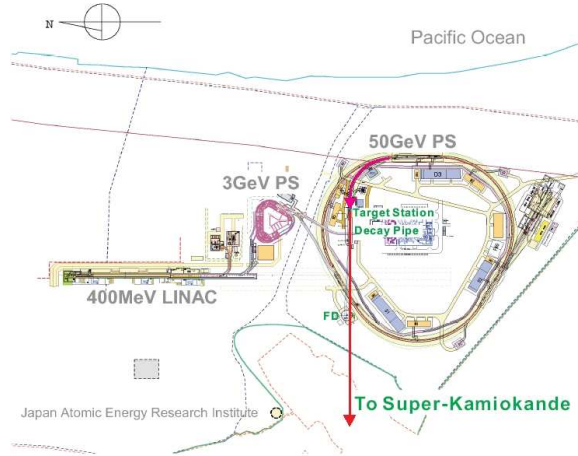


Figure 1: JHF site map.

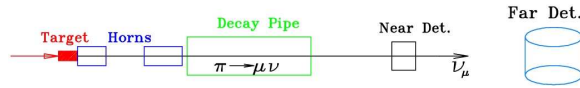


Figure 2: Path of beam from proton source to Super-K

2 The T2K Project

With the recent confirmation of neutrino oscillations, understanding the neutrino has become an important step in the progression of particle physics and the standard model. The T2K project aims to take this step by more accurately mapping out the oscillation patterns and energies of the neutrino.

The T2K project begins with the new 50 GeV proton synchrotron in Tokai and ends at the Super-Kamiokande 50kTon water Cerenkov detector in Kamioka. The proton beam is fired at a target which spews out pions and other associated debris (see figure 2). Magnetic focusing lenses called ‘focusing horns’ are used to focus only the pions into a beam. The pions then move down a decay pipe where they decay into muons and their counterparts, muon neutrinos. There is then a stopping block which allows only neutrinos to pass through, giving us our ν_μ beam. The beam immediately passes through a near detector 280m from the target, giving us initial beam readings, before traveling 295km to the Super-K far detector.

The Super-K detector is a gigantic cylindrical tank, has walls lined with

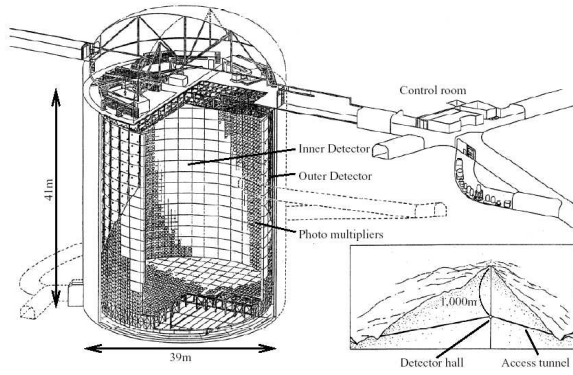


Figure 3: Super Kamiokande

11 200 photomultiplier tubes, and holds 50 kilotons of water(see figure 3). This provides a high density of neutrons with which the ν_μ beam can interact via the quasi-elastic neutrino scattering:



The recoiled muons coming from this reaction will emit Cerenkov radiation that can be detected by the PMT's and used to reconstruct the muons track. Now since this is a two body reaction, for each muon track there is only one possible proton track. With the track of the muon reconstructed, we are able to identify the energy of the incident neutrino and hence log a hit. Unfortunately, there are other neutrino scattering reactions that can happen which also have muons as products:



The muons from this reaction will also create a Cerenkov radiation signal, but these muons have less energy than the others as the pions must also carry some energy away from this reaction. Since this is a three body reaction and we can only reconstruct one of the product particles, we cannot use this data to reconstruct our neutrino energy. This creates a background to our useful muon signal; we must be careful not to confuse the two signals.

Although the 280m near detector does not yet have a completed design plan, its main purpose is to give more detailed information on the different neutrino interactions, as well as the initial beam composition. This information will help to analyse and interperate data coming from Super-K.

3 ND280m Design

The design of the 280m near detector is one of the main projects assigned to the Canadian Neutrino Group at TRIUMF. This detector will have many componets configured such that we can get the most information possible about the initial status of the ν_μ beam. This information is needed to analyse the data coming from Super-K and find out exactly how the beam is changing.

The component that I will be focusing on is a fine grained componet that will be able to track the recoiled protons from reactions shown in equations 1 and 2. Being able to reconstruct the protons as well as the muons we will be able to distinguish between the two reactions. With this we will be able to see the ratio of their relative occurence and project that onto the events logged in Super-K to remove the muon background. One problem is that this ratio is dependant on the material in which these reactions occur, and the scintillator material (CH) that will be used to track these protons is significantly different from the water (H_2O) used in Super-K. In order to reduce the systematic uncertainties caused by using different materials in these detectors, we plan to use a combination of both scintillator and water.

The current design plan for the fine grained component is to use thin layers of material, about 1cm thick, alternating water and scintillator. The layers are divided up into optically isolated bars, and arranged with them oriented orthogonally. Since the bars are optically isolated, a signal can be read out from each bar with a wavelength shifter fiber and a photomultiplier tube. Now if a track passes through two adjacent bars that are arranged orthogonally, we can narrow down its position quite well. On the other hand, if a particles track spends all of its time in one bar, we get very little useful information. Obviously the more bars a track hits the better we can reconstruct is energy and momentum, identifying the particle and the reaction that must have caused it.

In this particular study we are mainly interested in the geomerty of this detector, and the percentage of particles that will be trackable with a cost efficient segmentation. By running Monte Carlo simulations of this geometry, we will be able to see the precise energy and momentum spectra for which this level of segmentation will be sufficient for data reconstruction.

3.1 Cerenkov Radiation

When a particle enters a medium at speeds greater than the local speed of light in that medium, photons are emitted in the shape of a cone with half

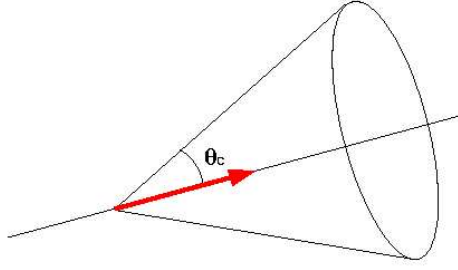


Figure 4: Cerenkov photons emitted in cone with half angle θ_c .

angle θ_c . The total number of photons generated, N , is a function of the particles energy and path length in the medium.

$$\theta_c = \arccos(1/n\beta) \text{ (where } \beta = v/c \text{)} \quad (3)$$

$$\frac{\partial^2 N}{\partial E \partial x} \approx C \sin^2 \theta_c(E) eV^{-1} cm^{-1} \quad (4)$$

In the case that our particles have constant energy, equation 4 simplifies to

$$N \propto C \cdot L \sin^2 \theta_c, \quad (5)$$

where L is the particle's path length.

3.2 Scintillators

Scintillators can be made with various organic and inorganic materials, taking on either liquid or solid form. The feature of a scintillator is that as radiation passes through it, its molecules get excited to higher energy states and then release radiation of their own as they return to ground states. This radiation is in the form of light, usually near the visible spectrum. One important characteristic of a scintillator is that it is transparent to its own radiation.

The scintillation energy generated is proportional to the energy deposited by the particle, with the additional quenching effect of the Burke's constant K_b .

$$\Delta E_{scnt} = \frac{\Delta E_{loss}}{1 + K_b(\Delta E_{loss}/\Delta L)} \quad (6)$$

$$N_{scnt} = C \cdot \Delta E_{scnt} \quad (7)$$

3.3 Wavelength Shifters

A wavelength shifter is a chemical whose molecules absorb light of one wavelength (and in turn one colour) and emit that light at another wavelength. This can be very useful in rendering invisible light (relative to the observer) visible. In this application, we consider plastic fiber of 1mm diameter containing wavelength shifters. The scintillation light is converted in the wavelength shifter fibers and transported to the photomultipliers.

3.4 Photomultiplier Tubes

The photon signal incident to the PMT (figure 5) strikes the photocathode, releasing photoelectrons (fewer than the incident photons). These electrons are then focused down a series of electrodes called dynodes. These dynodes are powered by an external voltage strong enough that each electron that hits will cause the release of several more. Thus the signal is multiplied as it travels down the chain of dynodes. One key feature of a PM device is that the gain is mostly determined by the voltage applied, and that this gain is constant as long as the voltage is stable.

4 Simulation Studies

4.1 Purpose

Recoiled protons from the charged current quasi-elastic neutrino scattering reaction (equation 1), are the most difficult particle that the 280m detector has to track. These protons will have momenta ranging anywhere below 1 GeV/c, with ranges in water and scintillator from 0-90cm. Now since the more hits we get from a track the easier it is to reconstruct, the obvious solution would be to make the segmentation of our detector as fine as possible. But as the segmentation gets finer, the number of wavelength shifting fibers and PMT's needed to read out a signal increases, as well as the cost

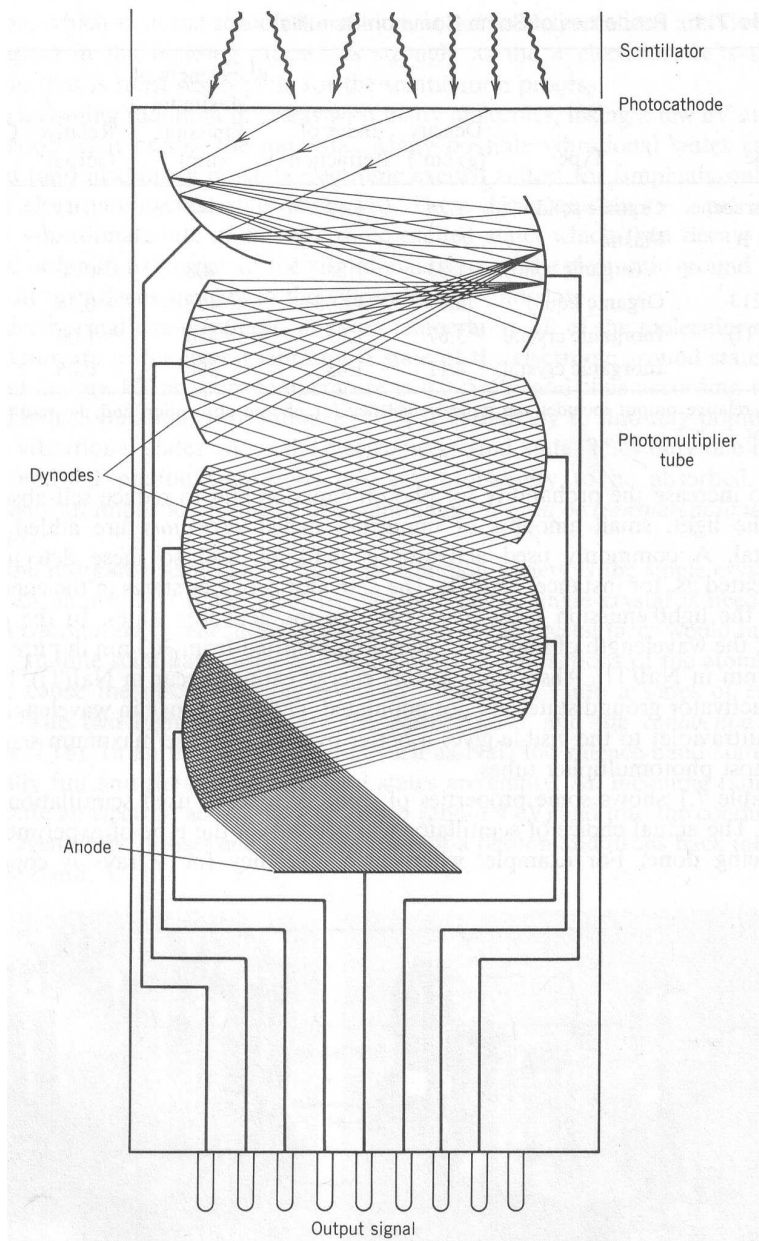


Figure 5: Photomultiplier Tube (PMT) Schematic from Krane, Introductory Nuclear Physics.

of our detector. This creates a point where it is no longer feasible to further increase segmentation.

Knowing how many hits we need to reconstruct our particles energies and paths, we can simulate proton paths through our detector at various expected momenta, and see how many hits we get for each. By doing this for a sample of 10 000 protons at each orientation in our geometry, we can get the mean number of hits and the percentage of particles that should be trackable at each orientation.

We can then use the quasi-elastic neutrino scattering equations to find out the probability that a ν beam of a certain energy will scatter protons at these specific angles and momenta. Combining this with the efficiency seen in the simulations, we should be able to see the probability of there being recoiled protons that we cannot track. This information will give us a better idea how fine we need to make the segmentation of our detector.

4.2 GEANT3 Configuration

GEANT3 is a powerful toolkit that was developed at CERN to simulate particle detectors' behaviour before building them completely. GEANT3 is built with Fortran77 and has libraries that know about most well understood physics interactions. The user writes code to define a specific detector geometry and material, simulate particle tracks, and output data. I have simply adopted and modified code, originally developed by Peter Gumplinger, to carry out the above mentioned studies.

The first thing that was done was to reconfigure the geometry definitions to focus on the geometry that we had in mind. To do this we added material definitions for water to the code, and set up the layers to alternate water and scintillator. The geometry also included definitions of a layer of wire chamber cells which we were not interested in. Instead of removing them altogether, the layers were simply configured so that there could be so many water and scintillator layers that the wire chambers are never encountered in our simulation. The dimensions of this geometry are set to give us 500 layers of scintillator and water (250 each) 3m x 3m and 1cm thick along the z-axis. The layers are divided up into 150 bars per slab, giving bars that are 1cm x 2cm x 3m with orientations alternating as shown in figure 6.

To ensure that our materials are behaving correctly, the simulated range of protons of various momenta were checked against the standard range data. By firing a proton beam straight into our detector for a series of initial momenta and fitting each sample for the mean range, we can plot these results against the ranges found in the TRIUMF Kinematic Handbook.

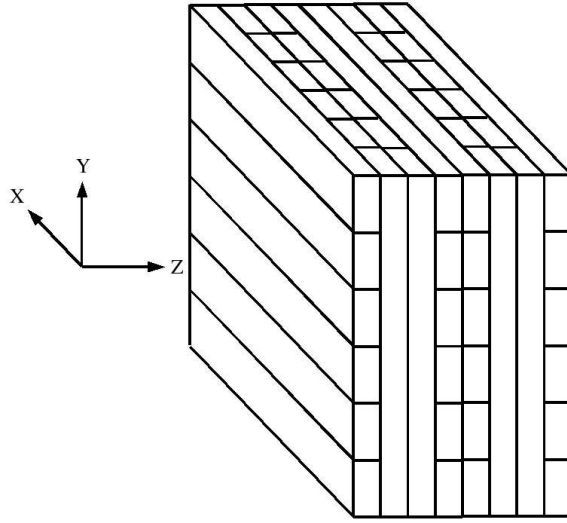


Figure 6: Detector composed of alternating slabs of water and scintillator. Each slab is divided up into bars, alternating in orientation.

Now, since our particles travel through water and scintillator layers, we take an average of the water and scintillator ranges found in the handbook. Although, our protons start in water and do not necessarily travel an equal amount in each material, but the effects of this are expected to be minimal. Considering the estimated error bars (although not shown), the plot shows sufficient accordance.

New code was also added to activate the production of Cerenkov photons. The code was modified so that the photons are not actually generated and tracked, but simply counted. To check these photon counts, we did a series of runs firing electrons into a slab of water for a series of initial momenta. From equation 4, you can see that the number of Cerenkov photons produced by a track requires the integration of the particle's energy over that track. To avoid this integration, we simply turn off energy loss so that our particles have constant energy over the entire track. The track length is also fixed, as the particle will always travel through the entire layer of water. Doing this, we can then fit our counts with equation 5. As you can see from figure 8, the simulated counts do follow the theory within statistical error.

Finally, some code was also added to produce scintillation photons. Again, the photons are only counted, not generated. It is actually equations 6 and 7 that are used by GEANT to sum the photon counts. They

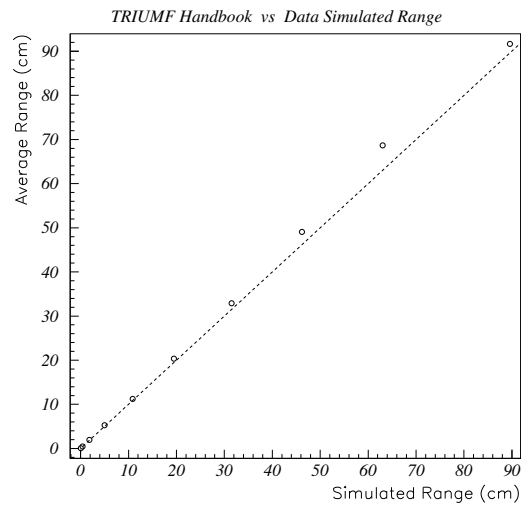


Figure 7: Simulated versus Experimental Ranges with 1:1 line

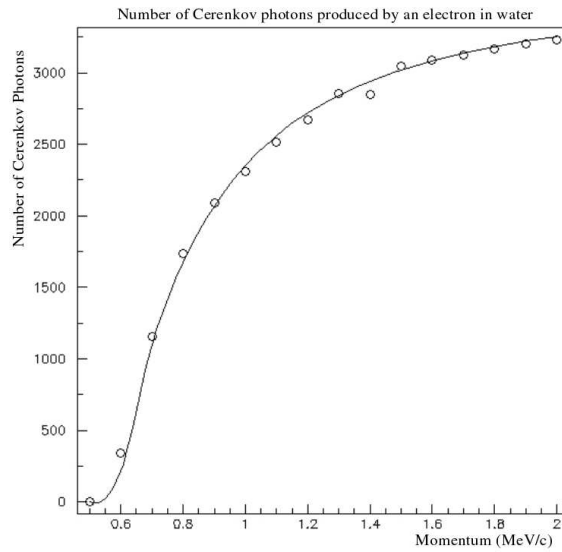


Figure 8: Simulated Cerenkov counts fit with Theory.

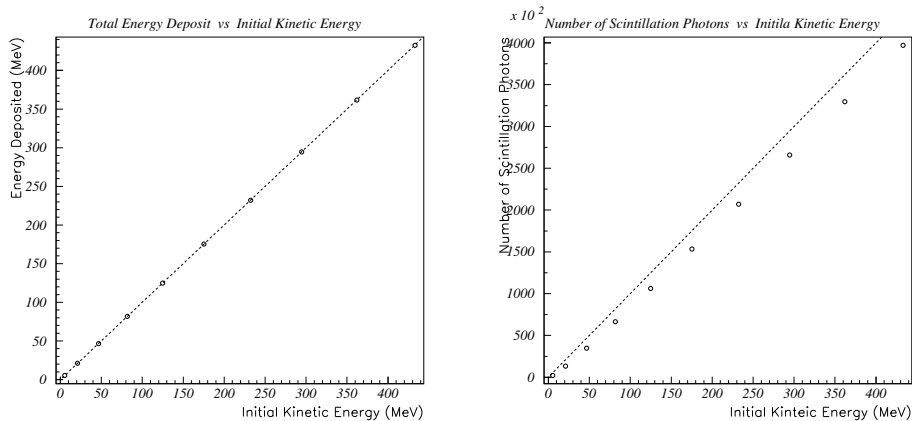


Figure 9: Energy deposit vs Initial Kinetic Energy with 1:1 line.

are integrated such that they update the counts at each step (GEANT step) in a particles track, giving the most accurate counts possible. Since this photon count is a function of the energy deposited by a track, we can compare these counts to the energy deposits and the initial kinetic energy of our protons. We should find that the energy deposited is equal to the initial kinetic energy, but that the photon counts are not directly proportional to the energy deposits, due to the effect of the Birkes' constant. We can see from figure 9 that the energy deposited is in fact almost exactly equal to the initial kinetic energy of our particles, and that the scintillation photon counts diverges in the anticipated direction.

4.3 Data Set 1

4.3.1 Setup

Now we want to run a set of simulations that will characterize the sensitivity of our geometry over all possible track orientations. Due to the symmetry of our detector about the z-axis, rotating our particle gun through angles in one quadrant of the xy-plane should be sufficient.

In this set of simulations the particle gun orientation is defined by 2 angles, θ_1 and θ_2 . θ_1 corresponds to rotation about the x-axis and θ_2 about the y-axis (as shown in figure 11). This set of orientations was generated by varying θ_1 from 0-80, and θ_2 from 20-80 with steps of 20° . At each orientation, runs were done for momenta ranging from 100-1000 MeV/c

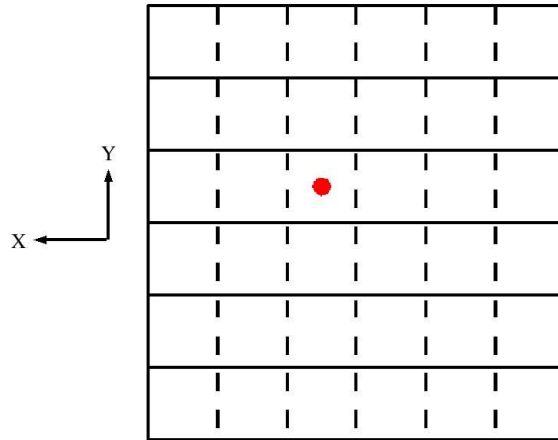


Figure 10: Origin of our particle gun.

with 100 MeV/c steps. This gives us a total of 200 runs, taking a single cpu over 2 days to process.

Also, the origin of our particle detector was set to the outer most edge (along z-axis) of the first layer, and centered in the square cross-section (in xy-plane) of two overlapping bars (see figure 10). The origin was centered in this way, to prevent particles from traveling along the boundary of two bars and giving confusing hit counts.

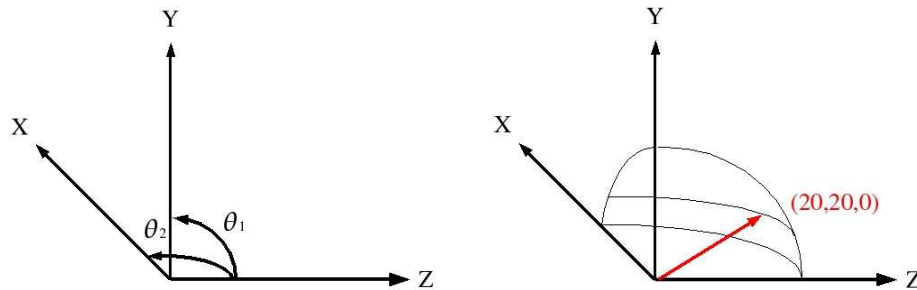


Figure 11: Orientation of particle gun in data set 1.

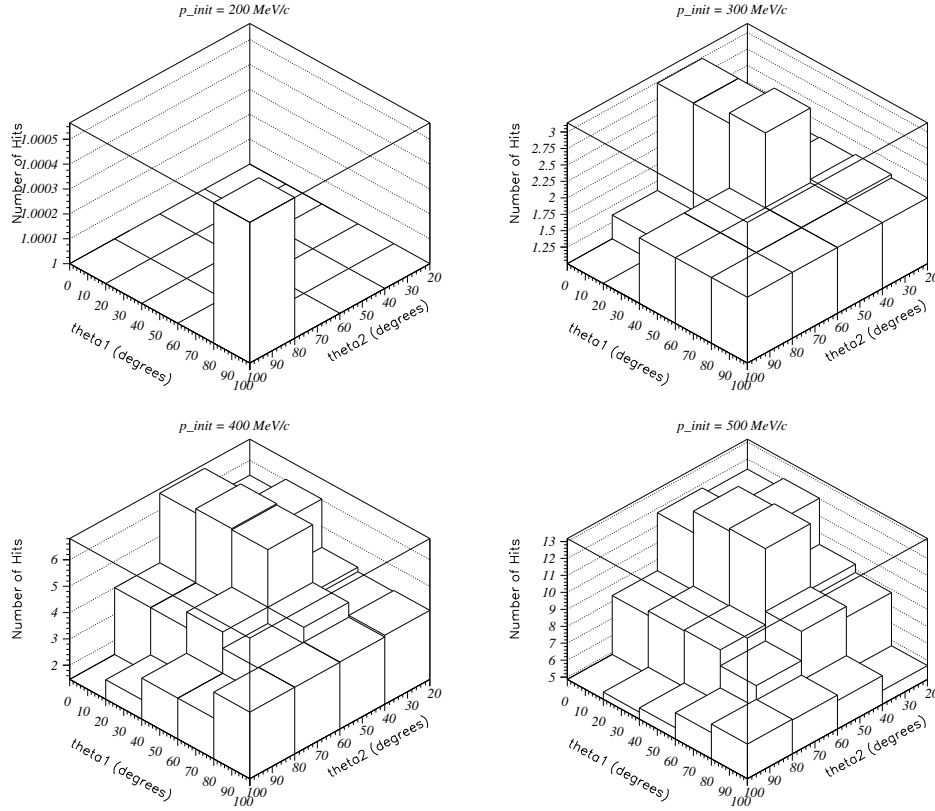


Figure 12: Number of hits for 200, 300, 400, and 500 MeV/c.

4.3.2 Results

We can now create 2-dimensional plots showing the mean number of hits as a function of θ_1 and θ_2 , for each initial momentum. The mean number of hits comes from a gaussian fit of our initial sample cut within 3σ of the mean range of each sample. By doing this we exclude protons that don't travel their full range because they go through nuclear interaction. This makes the variation in our hit counts (shown in figures 12 and 13) an effect mainly of the geometry and segmentation of our detector. Clearly the drop off in hit counts caused by the geometry happens at the higher θ 's, when the particles travel further down each bar.

Now since we want to know the percentage of events that will be trackable, we define an efficiency as the percentage of generated events that make at least a certain number of hits. Since we know that in order to get any

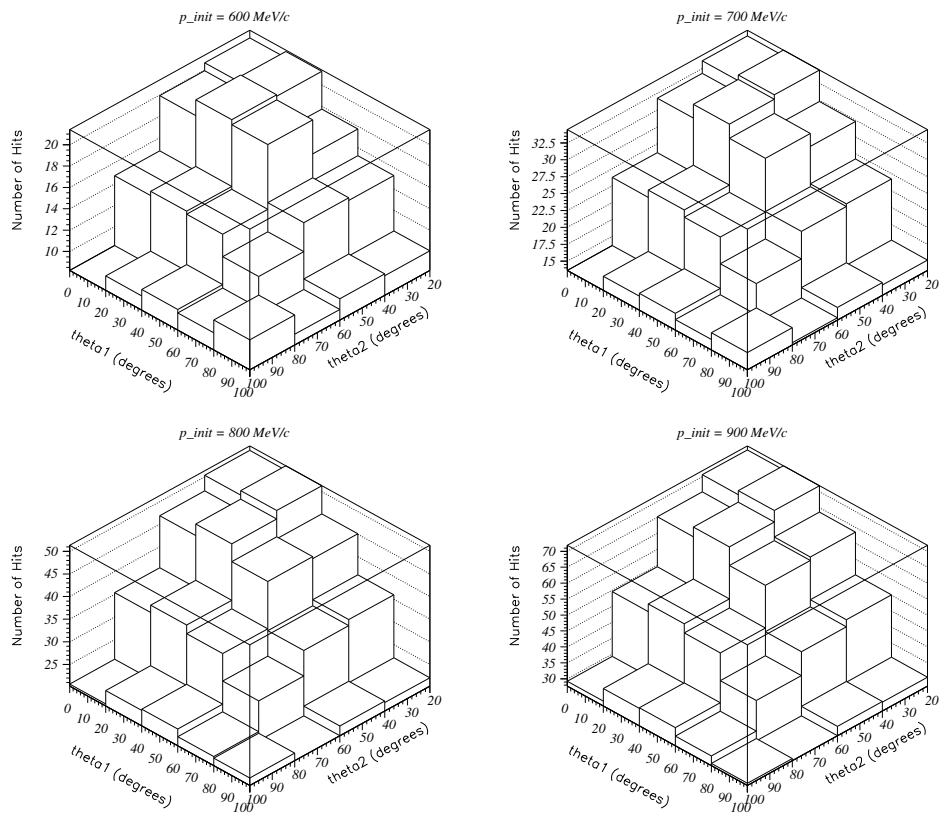


Figure 13: Number of hits for 600, 700, 800, and 900 MeV/c.

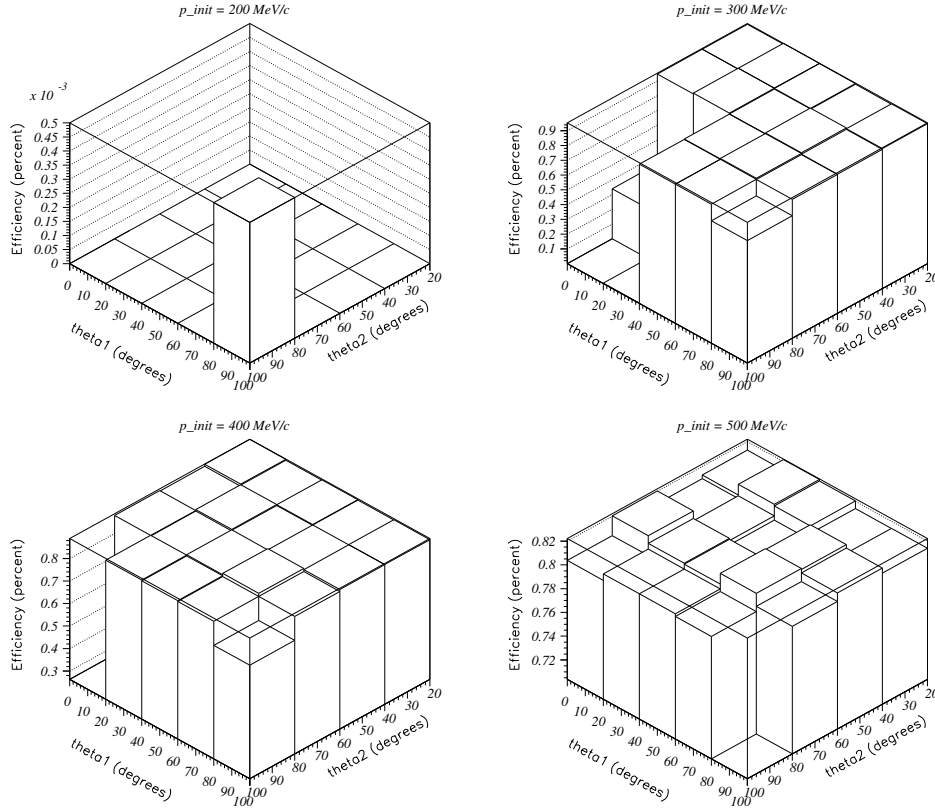


Figure 14: Efficiency at 2+ hits for 200, 300, 400, and 500 MeV/c.

valuable information from an event at least 2-4 hits are needed, efficiencies are defined for 2+, 3+ and 4+ hits.

Figures 14 and 15 show the 2+ hits efficiency as a function of θ_1 and θ_2 for different initial momenta. There is clearly a threshold momentum, between 200 MeV/c and 300 MeV/c for achieving 2+ hits with a reasonable efficiency. There is also a noticeable decrease in efficiency from 85% at 500 MeV/c to 48% at 900 MeV/c. This is the effect of the protons being stopped by oxygen nuclei as mentioned before. As the protons kinetic energy increases, the probability that it will hit a nuclei and stop also increases.

Figures 16 and 17 show the 3+ and 4+ efficiency plots. The same sort of trends are present with the threshold momentum now somewhere between 300 and 400 MeV/c

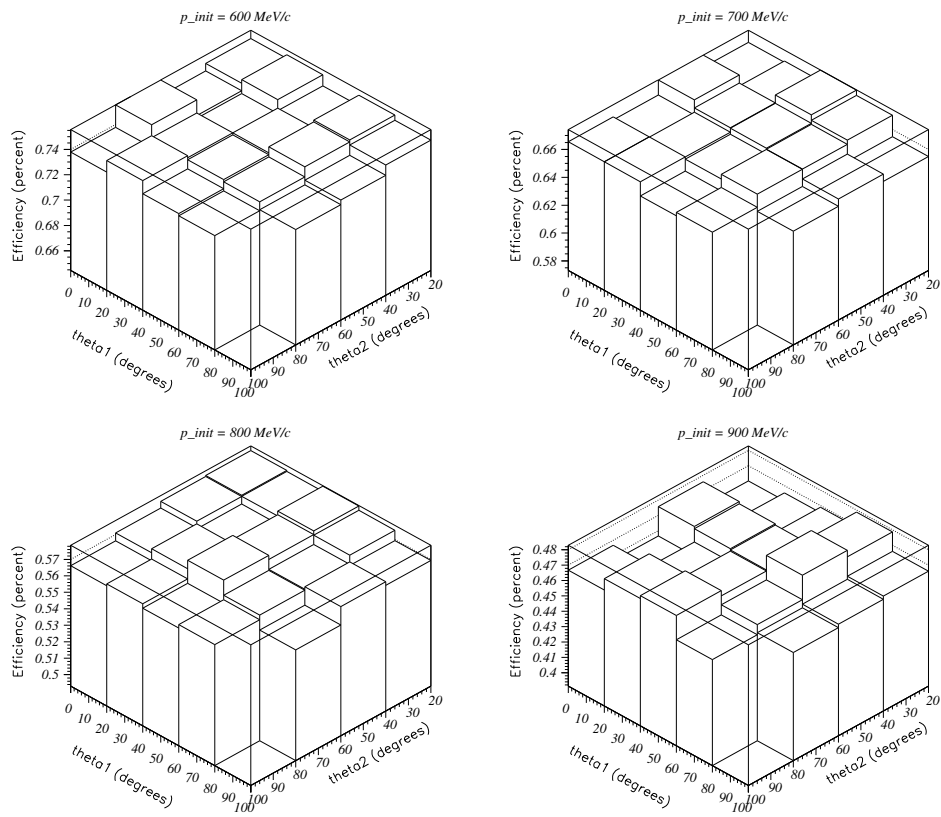


Figure 15: Efficiency at 2+ hits for 600, 700, 800, and 900 MeV/c.

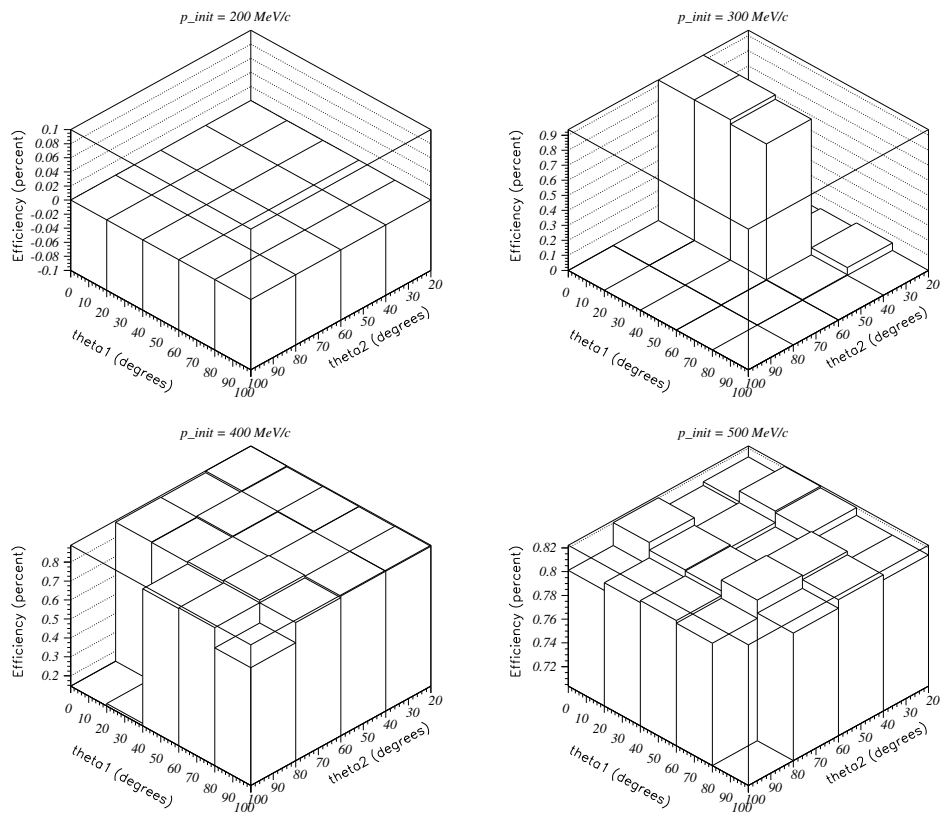


Figure 16: Efficiency at 3+ hits for 200, 300, 400, and 500 MeV/c.

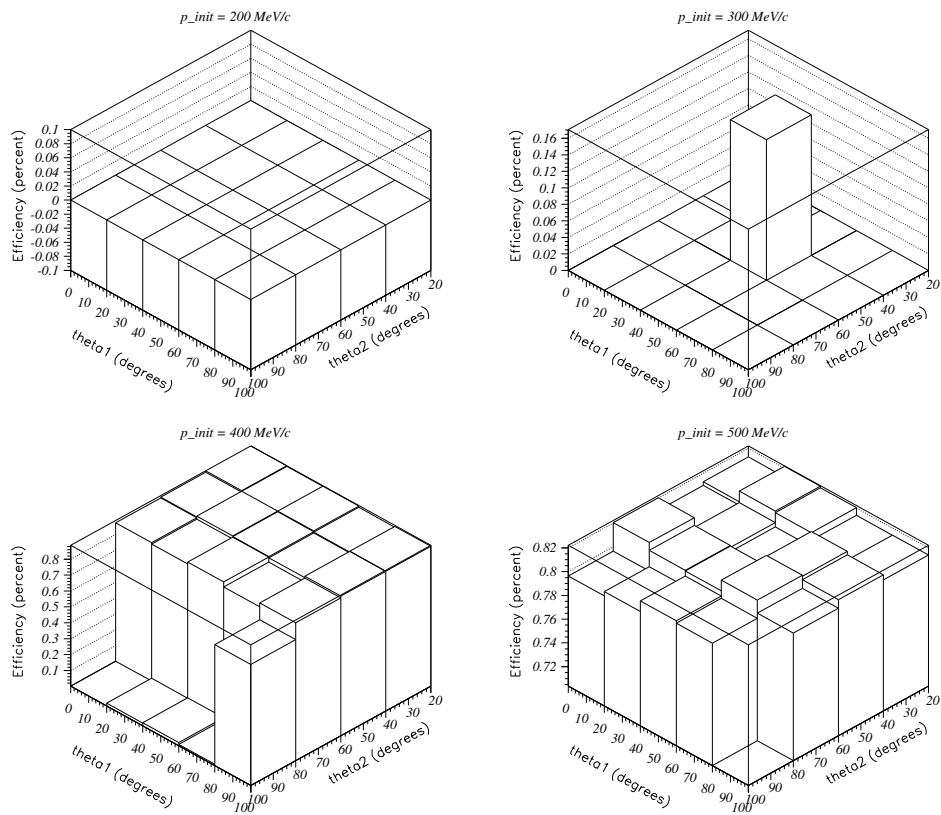


Figure 17: Efficiency at 4+ hits for 200, 300, 400, and 500 MeV/c.

4.3.3 Conclusions

From these figures it appears that protons of 200 MeV/c will almost never make 2 hits, protons of 300 MeV/c will almost always make 2 hits but never 3, and protons of 400+ MeV/c will almost always make 4+ hits. But this may not necessarily be the case. In these simulations, we had the origin of our proton beam fixed at the outer most edge of the first layer. This means that the protons must always pass through the entire first layer before making a second hit. On the other hand, in the real experiment these protons could originate anywhere inside the detector. This means that a 200 MeV/c proton could be generated just at the boundary of two bars, easily making 2 hits! We still know that a proton with a range of 0.4cm will only vary rarely be able to make 4+ hits with this segmentation, but this fixed origin may have a significant effect on our statistics.

In order to make this study as useful and accurate as possible, we must account for the various possible origins as well as track orientations in further simulations. It is also difficult to see exactly how the hit counts vary over θ with this resolution of sampled angles. In Data Set 2, we will also have a higher resolution of angles to get a better idea of the geometric effects of this segmentation.

4.4 Data Set 2

4.4.1 Setup

The first change made for this set of simulations is to create a distribution in the origin of our protons. By creating a linear distribution over the square cross-section from figure 10, as well as the whole first layer(along z-axis), we get an even distribution throughout the cube shown in figure 18. Although in the real experiment the proton origins will be distributed throughout the entire detector, with this distribution combined with the angular distribution in the one xy-quadrant, we should be accounting for almost every possible orientation a track could have in our detector.

In this set of simulations the direction of our proton beam is again defined by two angles, but not the same two as in Data Set 1. This is due to the distribution of the origin, which moves with the θ_1 and θ_2 of Data Set 1. This time θ and ϕ are used, and their behaviour is the same as spherical coordinates. In this case, θ is the angle between our particle track and the z-axis while ϕ is its rotation through the xy-plane, as shown in figure 19. Using these angles will also allow for an easier application of the scattering equations later on.

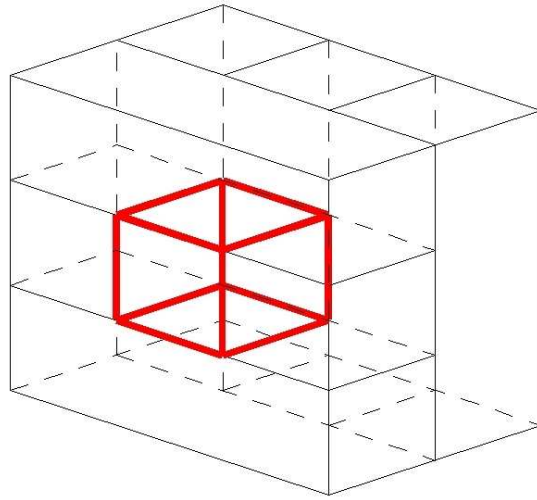


Figure 18: Cube in which particle origins are evenly distributed.

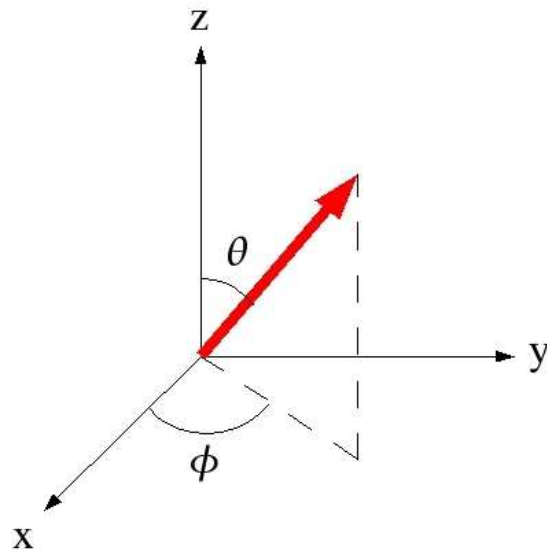


Figure 19: Coordinate system used for particle gun orientation in data set 2.

The resolution of angles sampled in this set has also been increased. Now we vary θ and ϕ through the full 0-90 degrees, with steps of only 5° . Also increasing the momenta sampled by decreasing the step size to 50 MeV/c, we get a total of 7220 simulations to be run! This amount of jobs could not be run on one cpu in any reasonable period of time, so we must make use of the westgrid computer facility. Westgrid is a network of cpu's with clusters spread across Alberta and British Columbia. We make use of a cluster of 1000 nodes called glacier, shared between SFU and UBC. For detailed documentation on the use of westgrid for a large number of jobs, see Appendix A.

4.4.2 Results

Looking at the new hit counts shown in figures 21 through 23, the high resolution of angles gives a much better idea of the geomertic effect of this detector segmentation. The point with the least amount of hits is at $\theta = 90$ and $\phi = 0$. These angles correspond to firing protons along the x-axis, where they will mostly stay within one water bar. You can see from figure 23 that even at the higher energies, the hit counts start to drop off significantly when $\theta > 30$, with a decrease of more than 60% from 30-90 degrees.

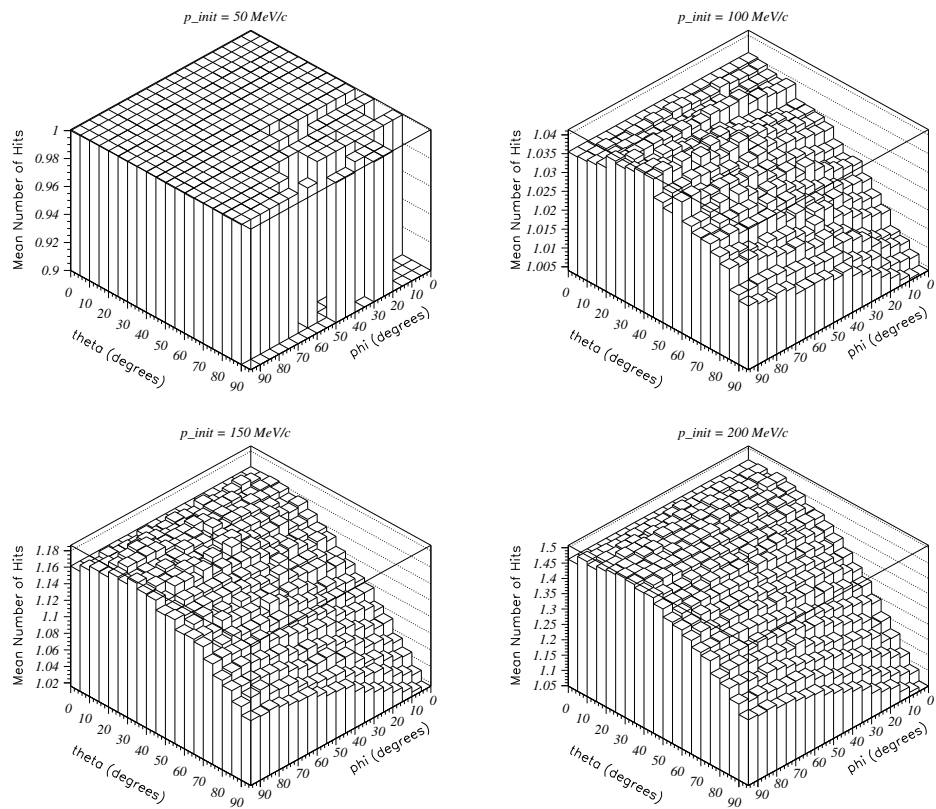


Figure 20: Hit counts for 50, 100, 150 and 200 MeV/c.

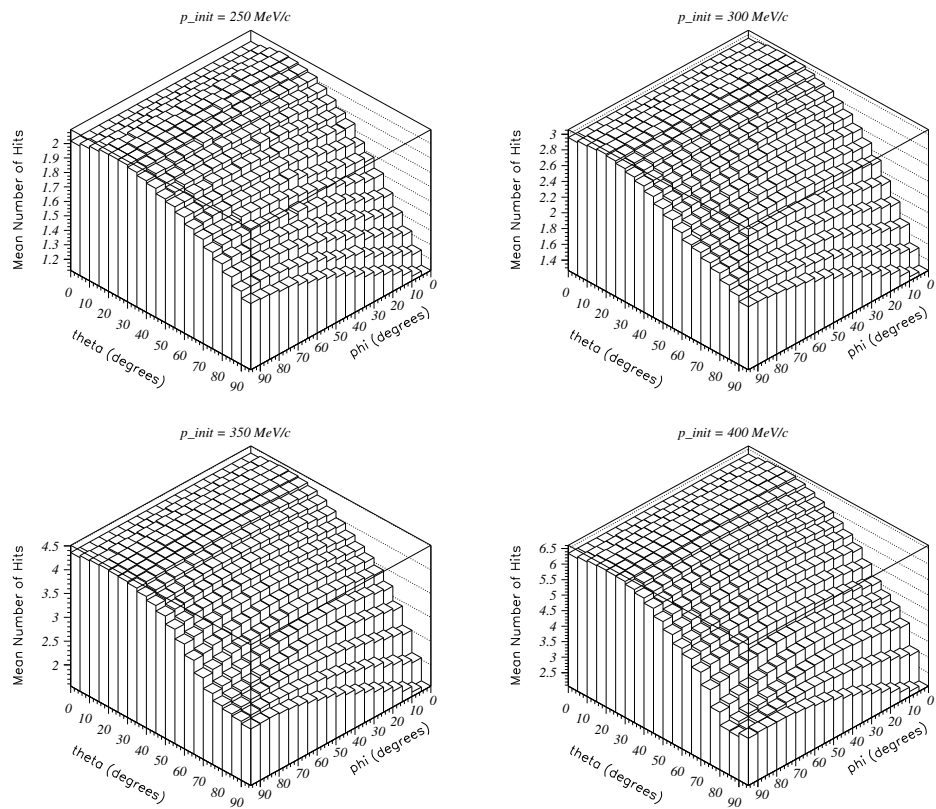


Figure 21: Hit counts for 250, 300, 350 and 400 MeV/c.

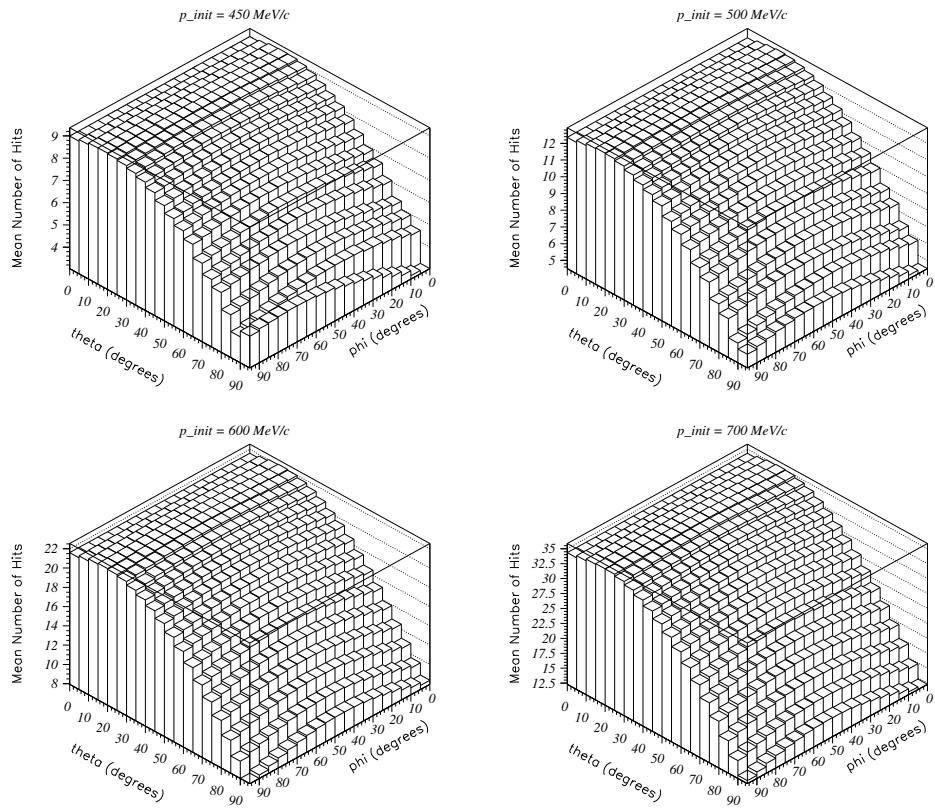


Figure 22: Hit counts for 450, 500, 600 and 700 MeV/c.

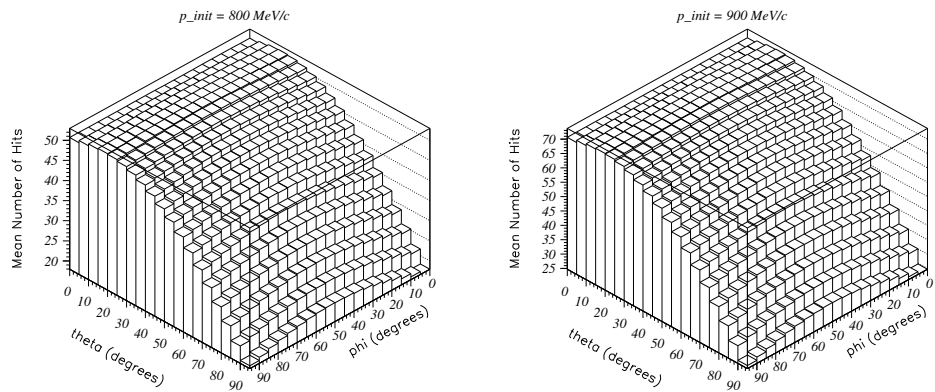


Figure 23: Hit counts for 800 and 900 MeV/c.

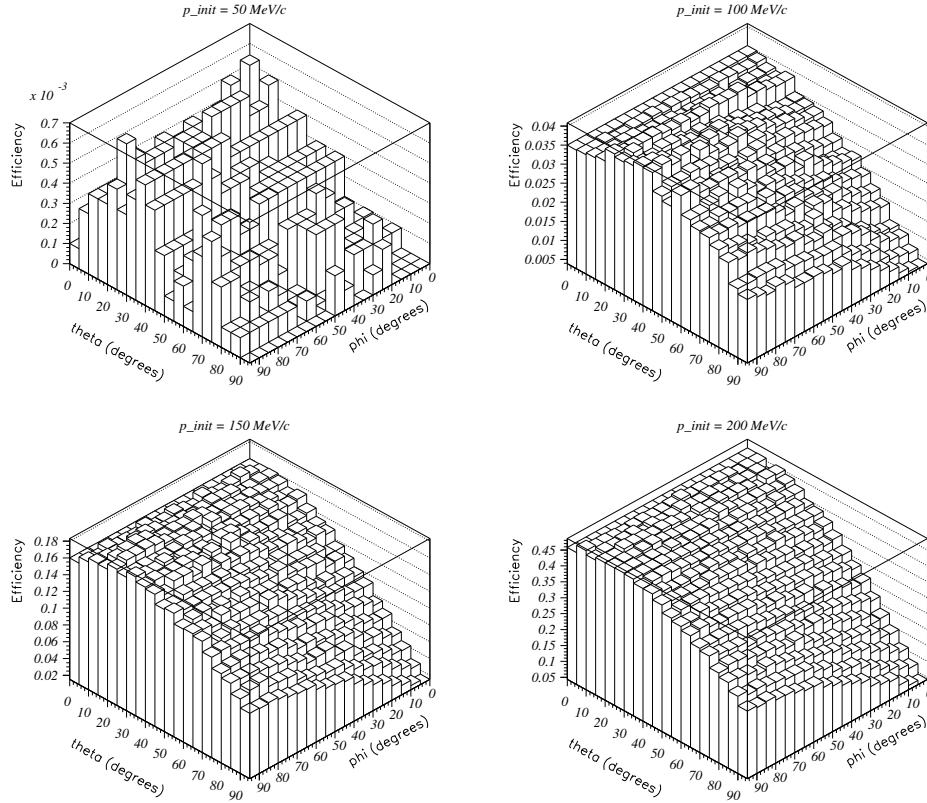


Figure 24: 2+ Efficiency for 50, 100, 150 and 200 MeV/c.

Since we are mainly interested in whether or not a track will be reconstructable, meaning it makes at least 2-4 hits, we can look at the efficiency plots. From figure 25 we see that we start to get a decent efficiency for 2+ hits around 250 MeV/c and can track almost all 300+ MeV/c protons. For 3+ and 4+ hits, our efficiency threshold is around 350 and 400 MeV/c.

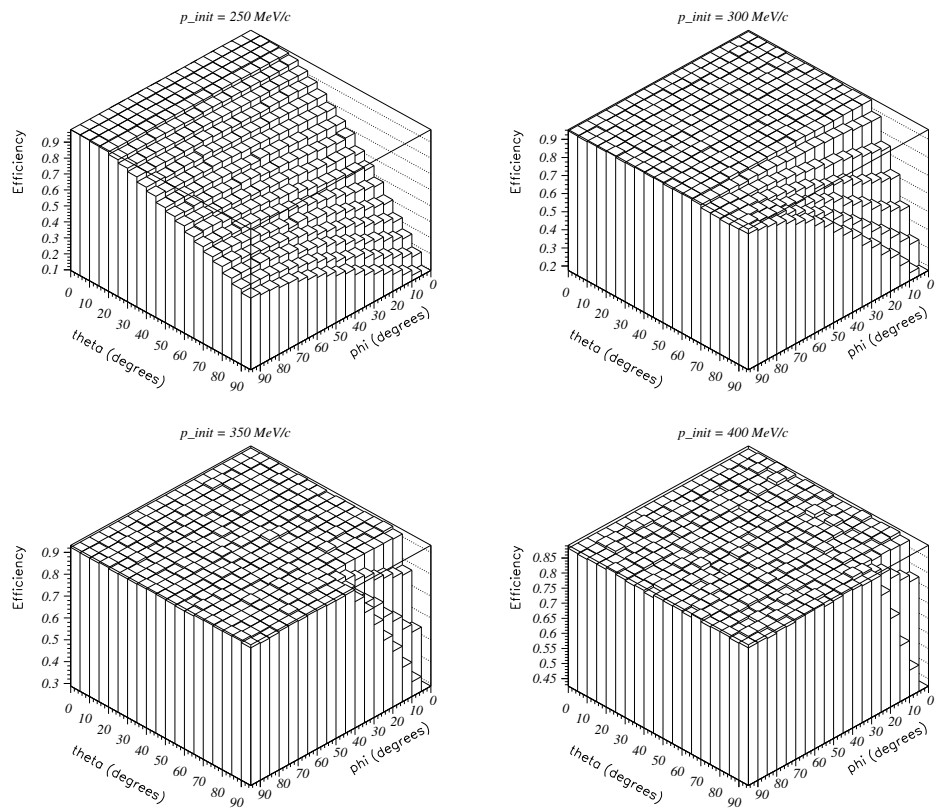


Figure 25: $2+$ Efficiency for 250, 300, 350 and 400 MeV/c.

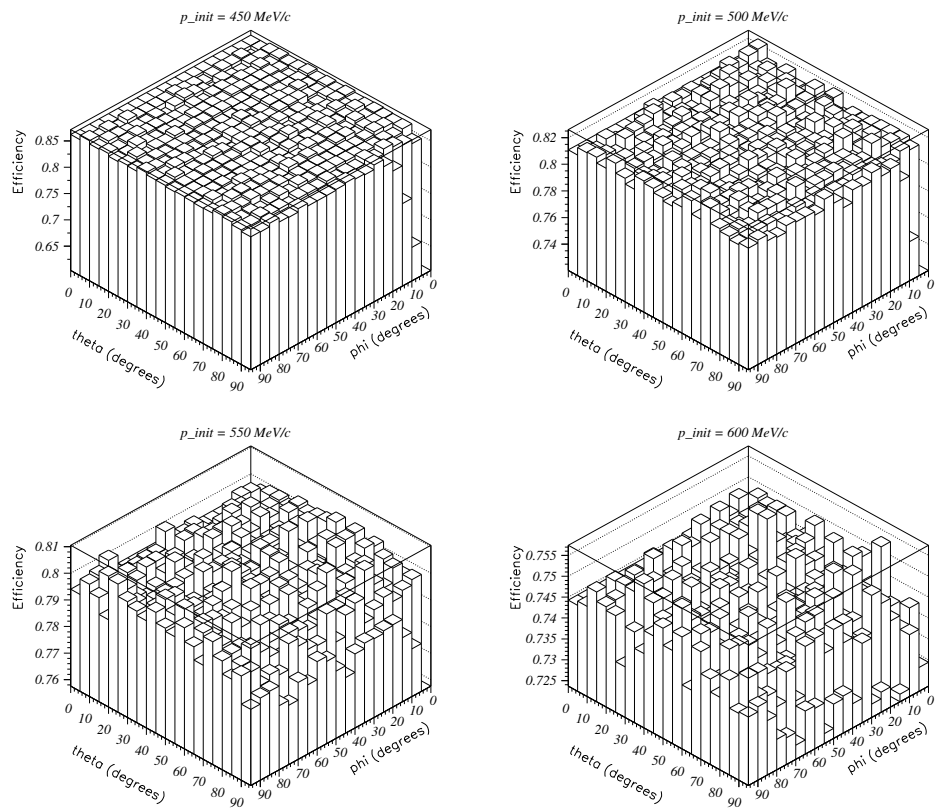


Figure 26: $2+$ Efficiency for 450, 500, 550 and 600 MeV/c.

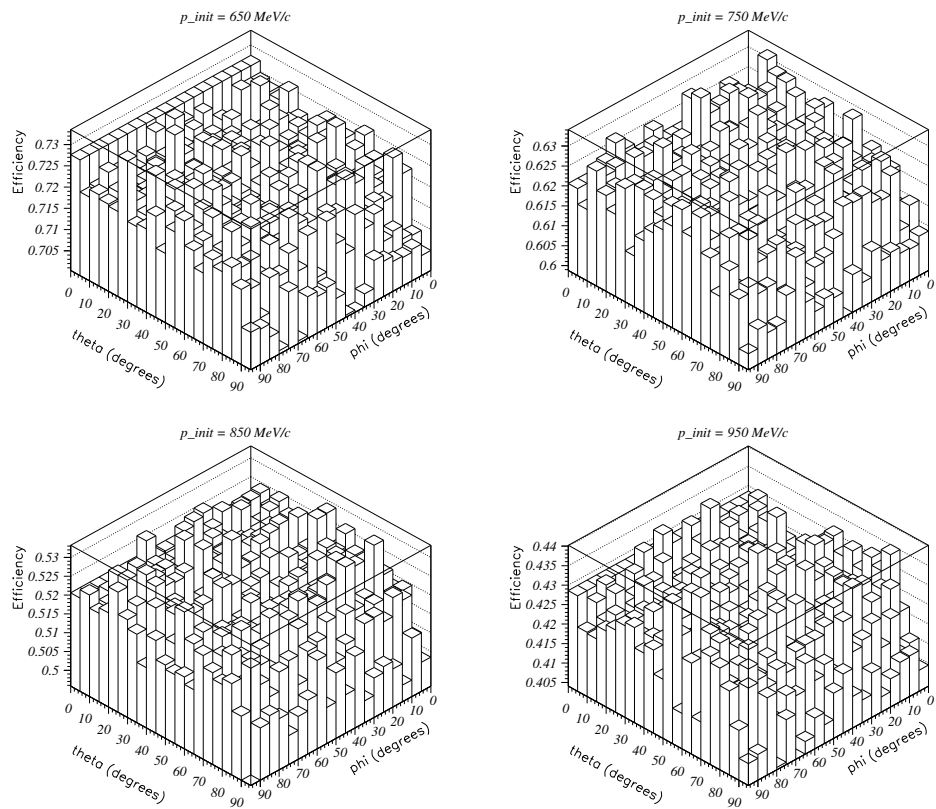


Figure 27: $2+$ Efficiency for 650, 750, 850 and 950 MeV/c.

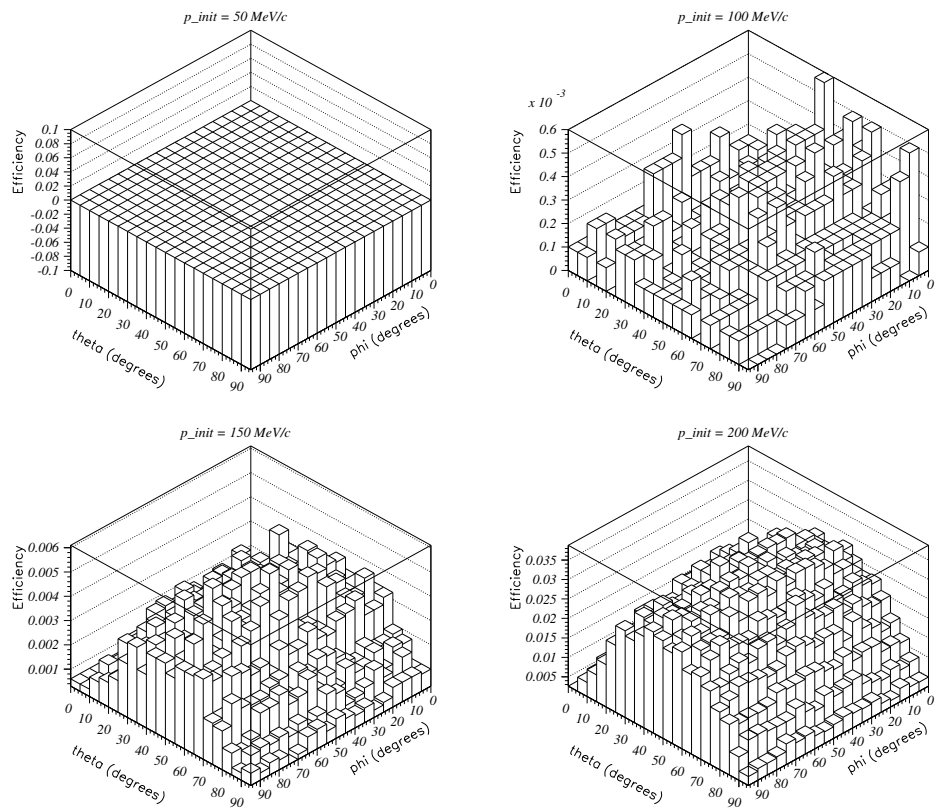


Figure 28: $3+$ Efficiency for 50, 100, 150 and 200 MeV/c.

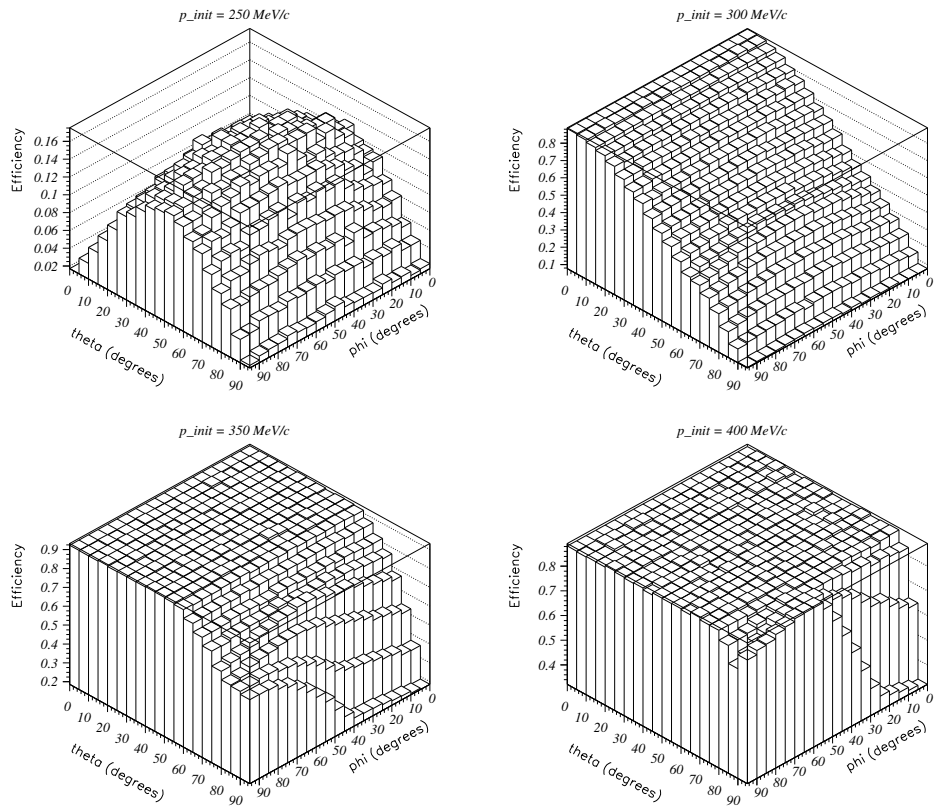


Figure 29: 3+ Efficiency for 250, 300, 350 and 400 MeV/c.

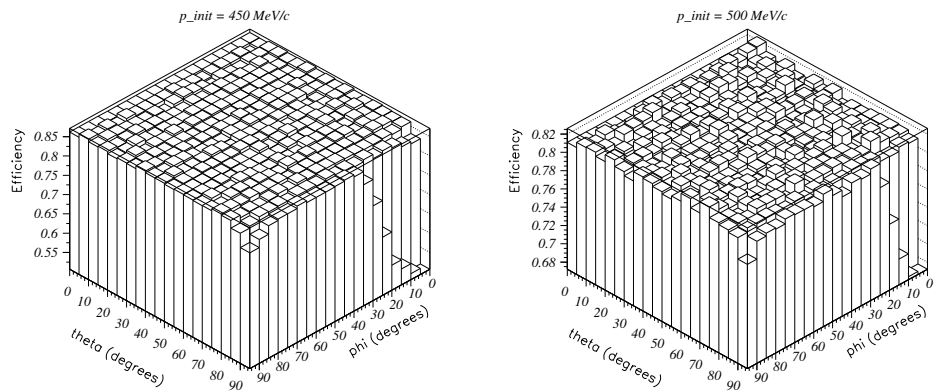


Figure 30: 3+ Efficiency for 450 and 500 MeV/c.

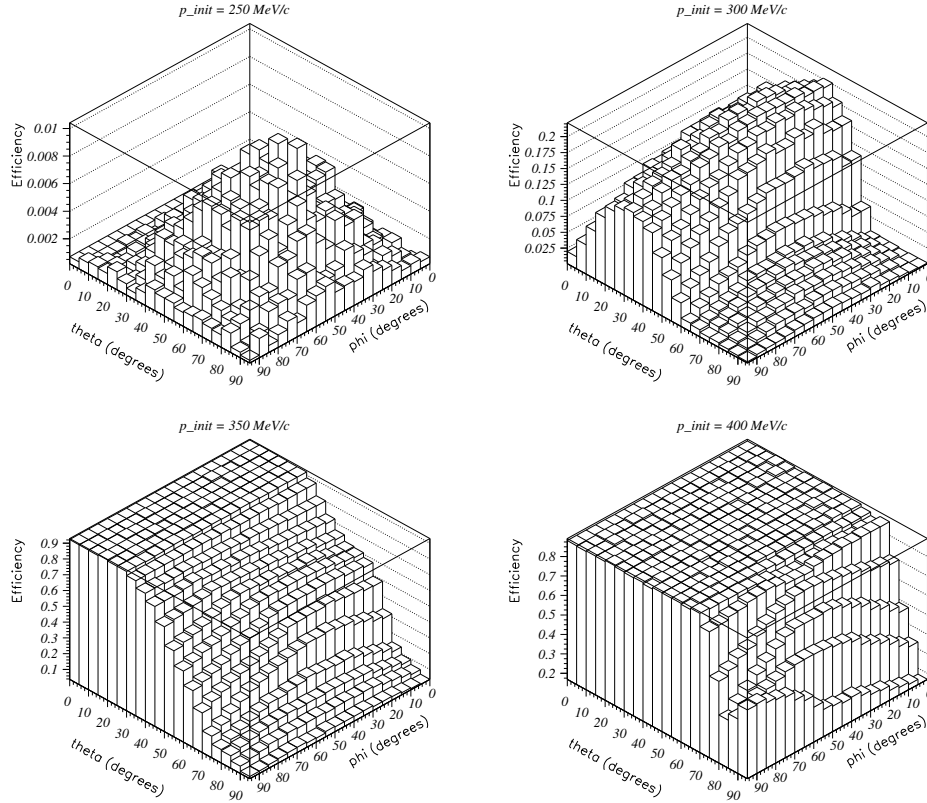


Figure 31: 4+ Efficiency for 250, 300, 350 and 400 MeV/c.

4.4.3 Conclutions

The higher resolution of angles sampled in this data set give a much more adequate view of how the hit counts and efficiencies drop off with θ . It looks like we should be able to do a full reconstruction for all protons over 400 MeV/c and at least a minimal reconstruction for most protons with at least 300 MeV/c. The question is now whether or not this will be a sufficient sensitivity for our near detector to have. To answer this, we need to know what angles we expect most of the recoiled protons to be scattered at. Clearly the efficiency of our detector decreases as θ increases. To see if this level of segmentation will really be sufficient, will will need to compare our efficiency results with a plot of the expected proton scattering angle distribution.

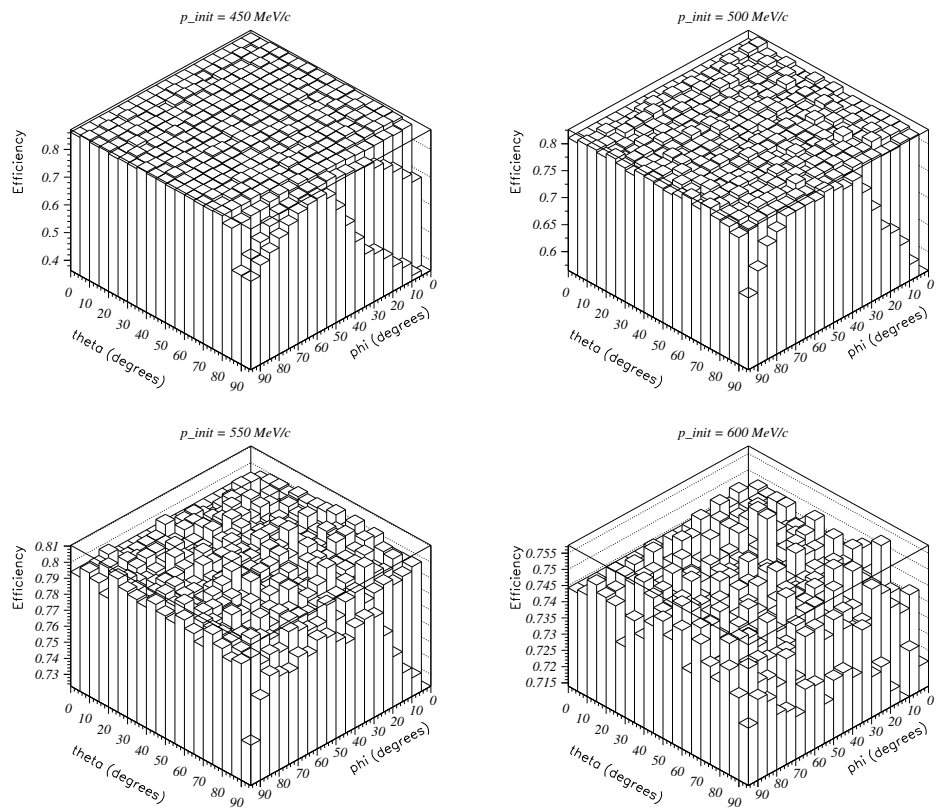


Figure 32: $4+$ Efficiency for 450, 500, 550 and 600 MeV/c.

4.5 Quasi-Elastic Recoiled Proton Distribution

4.5.1 Introduction

Now that we know the efficiency with which we will be able to reconstruct tracks of different orientations, we would like to know at what orientations to expect to see most often. Combining this information, we should be able to approximate the percentage of events that we will actually be able to see with this detector geometry and segmentation.

Since the Charged Current Quasi-elastic neutrino scattering from equation 1 is a two body reaction, for a given set of incident particle conditions, protons recoiled at a specific angle must have only one specific momentum. For this set of recoiled proton momenta, there is a distribution of the relative probabilities that any one will occur. The sum of these probabilities must of course be one, as a recoiled proton must have a momentum in this finite set. To generate this distribution of probabilities we must make some assumptions in choosing our set of initial conditions.

First we can make some assumptions about our neutrino beam. We will say that it is a mono-energetic beam travelling straight along the z-axis. Of course neither of these are entirely true as there will be some distribution to the angles and energies that our incident neutrinos have, but for the bulk of events it should be sufficiently accurate. We will also have to make some assumptions about our target neutrons. In this case we assume that we have a stationary target full of neutrons hovering at rest, ignoring the Fermi motion of the neutrons inside the nucleus. Although this is a well known phenomenon, its effect on our results compared to the time it would take to incorporate did not make it feasible at this stage of study.

With these assumptions now in place, it would seem that there is only one possible outcome. But this is not simply a two-body kinematics problem. The structure of the target nuclei is quite significant. This is why it is so important that the target used in the near detector be as similar as possible to that used in the far detector. The effect of the nuclear structure on particle scattering is described by something called a form factor, a mathematical device based on extensive empirical data. As my understanding of form factors is significantly inadequate at this point, I will not attempt to explain them in any more detail here. Some code was put together by Stan Yen to produce the information I required.

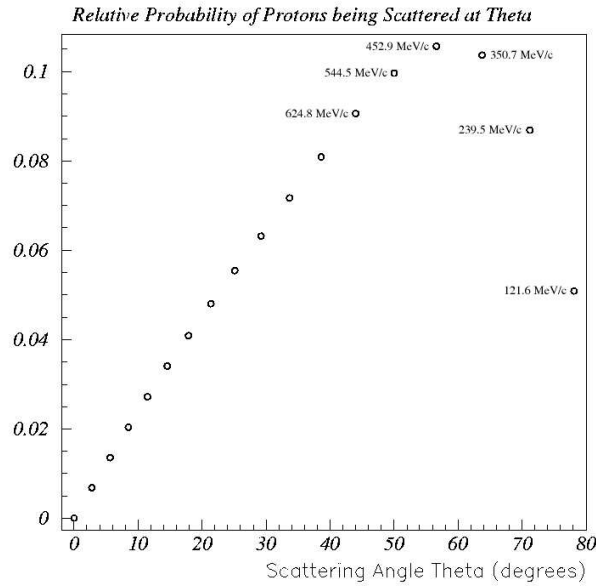


Figure 33: Distribution of recoiled proton probabilities for ν_μ beam of 700 MeV.

4.5.2 Results

Data was generated describing the relative probabilities of recoiled protons being scattered from an incident neutrino beam of 700 MeV. 18 scattering angles were sampled, spanning the entire range of possibilities. In figure 33 we see that the majority of our recoiled protons will be scattered between 50-70 degrees from the z-axis. As each one of these scattering angles can only have one proton energy associated with it, I have label some of the crucial points with their associated momenta. Now our detector is most efficient at smaller scattering angles and higher proton energies, the bulk of protons will be scattered at higher angles, and that as the scattering angle increases the proton energy decreases! This creates a point where the energies get too low and the angles get too high, and we will no longer be able to track these protons.

Now to find out the percent of these protons that will be trackable, we need to compare the results from figure 33 with the efficiency tables generated earlier. But the efficiency of our detector varies significantly over ϕ , and the scattering angle probabilities do not mention ϕ at all. In fact

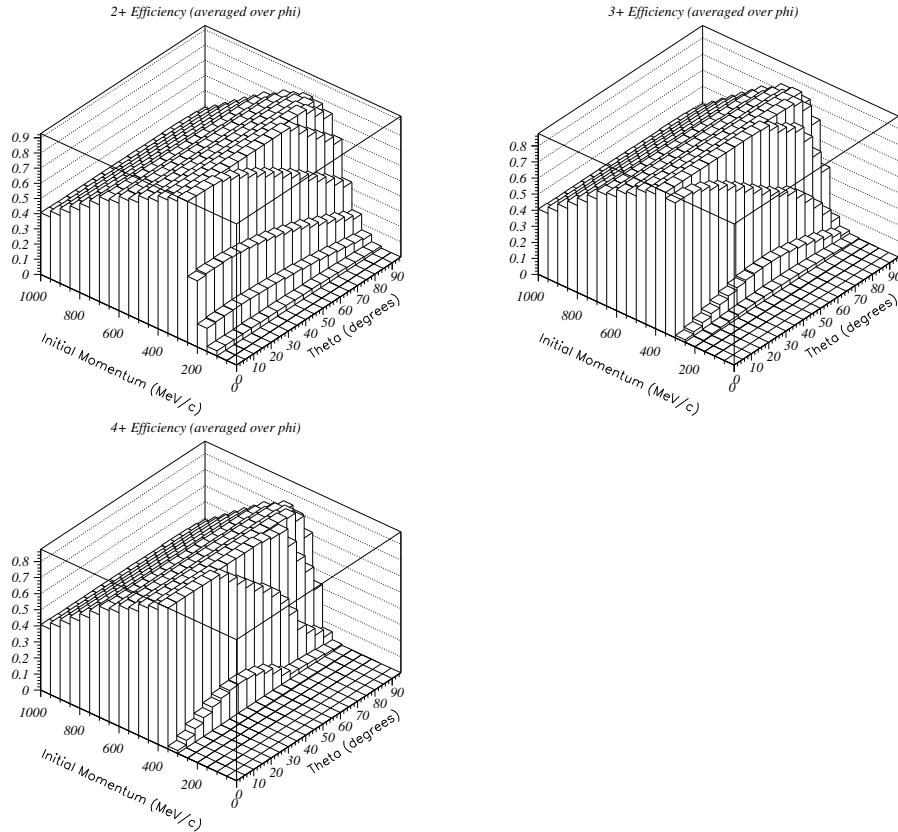


Figure 34: Efficiency as a function of initial momentum and θ for 2+, 3+ and 4+ hits.

the scattering equations predict an completely even distribution through all angles of ϕ . Therefor, to make this comparison easier I have taken the previous efficiency plots and averaged them over ϕ . This gives us three new efficiency plots of efficiency as a function of initial momentum and θ , one for 2+, 3+ and 4+ hits.

By taking each point from figure 33, and multiplying the percentage of events scattered at that angle by the efficiency of tracking it predicted by figure 34, we can then sum all these reduced percentages to get the total percent of scatterings that will be trackable. Unforutnately since even protons scattered at low angles with high momenta don't often travel their full range before being stopped by nuclei, these results are surprisingly low. It is calculated that we will only be able to do full reconstruction of 53% of

events, and at least partial reconstruction of 62%.

4.5.3 Conclusions

After combining the scattering probability distribution with our efficiency information, it appears that we will only be able to partially reconstruct 62% of our protons, and fully reconstruct 52%.

One significant assumption is that any protons that travel less than 3σ below the mean range of protons with that energy will not be reconstructable. If we did on the other hand assume the same level of reconstructability for these as the rest of our protons, we would get predicted values of 70% and 80% reconstructability. In these simulations, we do not look at the electromagnetic showers and energy deposits made by these protons, so I cannot say whether or not they may be reconstructable. This may be worth considering.

4.6 Summary of Conclusions / Recommendations

For an incident ν_μ beam of 700 MeV, we should be able to fully reconstruct 50% of events and partially reconstruct 60% of events. There are of course many assumptions made in this study and to really understand these values, we must consider each of these assumptions, why they were made and the effect they may have had on our results.

One significant factor is that in our efficiency plots, we consider all protons that do not travel within 3σ of their expected ranges to be untrackable. This is not entirely true, as many of these tracks will still make well over 4 hits before they are stopped. What should have been done was to look at the percentage of these protons that make more than 4 hits. I would expect this number to be at least 90%! If we do consider these tracks to be fully reconstructable like any other that makes that many hits, we get 70% and 80% full and partial reconstructability respectively. I would consider these numbers to be a realistic idea of what would be possible geometrically, but we really must consider the characteristics of the signal and our ability to detect.

First of all, the efficiency plots describing this detector geometry are based solely on the number of hits made by a track. In this simulation GEANT records a hit for any bar in which at least 1 keV of energy is deposited. It also does not consider the efficiency with which a wavelength shifter fiber and photomultiplier tube will be able to read out a signal. The actual light transmission of our materials and the efficiency of our PMT's

will lower the ideal geometrical efficiencies calculated from the simulation.

The other problem with this simulation is that we do not look at our data in the same way that we would in the real experiment. In the real experiment all we will have to look at is the signal strength and timing that we get from our array of PMT's. These signals will also be clouded by signals from the recoiled muons as well as other reactions that will be occurring. Even if we do have a proton track with a sufficient number of hits to be reconstructed, there may be signal interference from another nearby reaction. To consider we could look at the output of neutrino interaction generators, such as NEUT or NUANCE, and look at the particle showers produced and their approximate signals.

If we momentarily disregard the relative amount of light needed to read out a signal, along with the signature of the signal and expected background, we have a study focused on the optimal geometry for our detector. One important factor in this study is the angles and energies with which we expect the protons to be scattered. This was calculated giving the plot in figure 33, but we do make some assumptions about the physics involved here. Most importantly is the consideration of the Fermi motion of the nucleus. It has been anticipated that this consideration may smooth out the lower energy points in the plot in figure 33. Also, if we consider our ability to reconstruct high energy protons that make more than 4 hits but go through have strong hadronic interactions, we will be able to tell in which direction our most troublesome particles will be travelling.

There is one final idea that I had. If we do in fact find that the more difficult particles that we need to track is more in the x and y directions, we should consider rotating the detector 90° about the y-axis. This would align its more efficient axis with the direction we expect our short range protons to be traveling. This would cause no engineering changes and could be simulated quite easily. If we consider the directions and energies of other particles creating signals in our detector, we could see if this rotation would be a significant improvement.